

Electrical control of ultrafast intra-molecular dynamics in an artificial molecule

K. Müller,¹ A. Bechtold,¹ C. Ruppert,² M. Zecherle,³ G. Reithmaier,¹ M. Bichler,¹ H. J. Krenner,⁴ G. Abstreiter,¹ A. W. Holleitner,¹ J. M. Villas-Boas,⁵ M. Betz,² and J.J. Finley^{1,*}

¹*Walter Schottky Institut and Physik-Department,*

Technische Universität München, Am Coulombwall 4, 85748 Garching, Germany

²*Experimentelle Physik 2, TU Dortmund, 44221 Dortmund, Germany*

³*Physik-Department E11, Technische Universität München, James-Frank-Str, 85748 Garching, Germany*

⁴*Lehrstuhl für Experimentalphysik 1 and Augsburg Centre for Innovative Technologies (ACIT), Universität Augsburg, Universitätsstr. 1, 86159 Augsburg, Germany*

⁵*Instituto de Física, Universidade Federal de Uberlândia, 38400-902 Uberlândia, MG, Brazil*

(Dated: July 29, 2022)

We employ ultrafast photocurrent spectroscopy to directly probe the tunneling of charge carriers in a single, electrically tunable self-assembled quantum dot molecule. Pronounced anticrossings are observed arising from tunnel couplings between different electronic orbitals in the two dots. Time-resolved photocurrent measurements performed in the vicinity of these anticrossings provide direct information on few Fermion tunneling dynamics, the transient optical response of the molecule and both, elastic and inelastic intra-molecular tunneling. The intra-dot electron tunneling time and its dependence on energy detuning are directly probed with times as short as ~ 5 ps observed close to resonance. A strong asymmetry in the detuning dependent tunneling time is observed from which phonon-assisted inelastic tunneling is shown to be most efficient for energy detunings of ~ 1.7 meV, reflecting the spectral function of the molecular exciton-phonon coupling.

Tunneling is a widespread phenomenon in both low- and high-energy physics. For example, it governs the dynamics of nuclear decay, tunnel ionization of atoms and vertical electron transport in semiconductor heterostructures. In all of these systems tunneling generally occurs to and/or from a *continuous* distribution of initial or final quantum states associated with particles having one or more motional degrees of freedom. However, tunneling between discrete quantum states in solids having a specific energy separation is of particular interest since additional quasiparticles may be required to ensure energy conservation. Semiconductor nanostructures are an ideal testbed for such processes since energy levels can be arbitrarily designed whilst coupling to the phonon bath can facilitate inelastic tunneling. So far, inelastic tunneling between fully localized states has been studied only indirectly by transport measurements in electrostatically defined double quantum dots (QDs) [1, 2] and in locally gated carbon nanotubes [3]. In strong contrast, self-assembled QDs offer the advantage of strongly localized electron and hole states and the possibility to perform time-resolved *optical* and *optoelectronic* measurements to directly monitor carrier populations in real time. In addition, vertically stacking of optically active QDs produces artificial molecules with strong, electrically switchable dot-dot tunnel coupling. Such tunnel couplings occur when quantum state are tuned into resonance and are manifested as pronounced anticrossings in optical experiments [4–6]. Tunnel coupling occurs for either electrons or holes [7], depending on the relative dot size and couplings between different orbital states can occur due to symmetry breaking [8]. Whilst photoluminescence (PL) measurements have revealed a large tuneability of static

properties, such as Landé g-factors [9, 10] or spin dependent couplings (singlet-triplet splittings) [5, 11], dynamic properties can only be indirectly studied by comparing data with models [12, 13]. The impact of tunnel coupling on the ultrafast intra-molecular carrier dynamics remains practically unexplored.

In this paper we report direct investigations of the few Fermion spectra and intra-molecular dynamics in a single QD-molecule (QDM) formed by strain driven self-assembly [4]. Picosecond pump-probe photocurrent (PC) spectroscopy is employed to directly probe the tunneling dynamics of electrons and holes in the system. The intra-dot electron tunneling time is directly measured and its dependence on the energy detuning of orbital states in the two dots forming the molecule is traced. Close to zero detuning ultrafast resonant tunneling is observed (~ 5 ps), with strongly asymmetric tunnelling times for non-zero detunings. This is shown to arise from inelastic (phonon mediated) intramolecular tunnelling allowing us to directly map out the spectral function of the exciton-phonon inelastic tunneling rate. Inelastic tunneling is shown to be most efficient for energy detunings of ~ 1.7 meV, reflecting the spectral function of the molecular exciton-phonon coupling strength. This model is supported by temperature dependent measurements and theory.

The sample consists of a vertically stacked pair of self-assembled InGaAs QDs separated by a 10 nm thick GaAs spacer and embedded within the intrinsic region of a GaAs Schottky photodiode. It permits complementary PC and PL measurements by varying the applied voltage. For the QDM investigated in this study we observe a pronounced anticrossing in PL experiments with a cou-

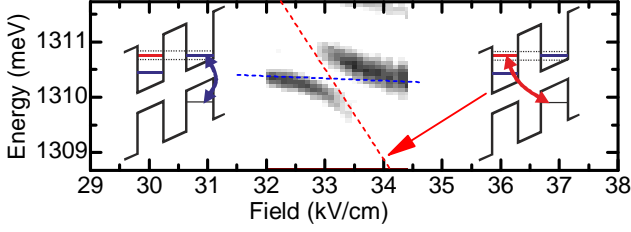


FIG. 1. (Color online) Anticrossing related to tunnel coupling of the electron in the ground state of the upper dot and an excited state of the lower dot.

pling strength of $2V_0 = 3.4 \text{ meV}$ at an electric field (F) of $F_0 = 23.1 \text{ kV/cm}$ (not shown - see ref [14]). This anticrossing arises from a coupling of direct and indirect neutral exciton transitions where the hole is located in the upper QD and the electron located either in the lowest orbital state in the upper dot (e_{ud}) or lower dot (e_{ld}), respectively. As the electric field increases the PL signal quenches due to tunneling escape of electrons and holes from the dot and the direct exciton in the upper dot can be monitored in PC-experiments. As presented in Fig.1, this direct exciton exhibits a second, weaker anticrossing at $F_1 = 33.1 \text{ kV/cm}$. The splitting at resonance is $2V_1 = 0.8 \text{ meV}$, significantly weaker than $2V_0$, indicative of weaker coupling. We identify the second anticrossing as depicted schematically in the inset of Fig.1; the lowest electron level in the upper dot (e_{ud} - blue arrow, Fig.1) is tuned into resonance with an excited orbital electron state in the lower dot (e_{ld}^* - red arrow). The resulting coupling is $V_1/V_0 = 4.25$ times weaker than the principle anticrossing at F_0 since the in-plane parity of the coupled states have different parity; s-like for e_{ud} and p-like for e_{ld}^* . The difference between the two electric fields where the two anticrossings occur $F_1 - F_0 = 10.0 \pm 0.1 \text{ kV/cm}$ can be used to estimate the energy separation ΔE of the two electron levels in the lower dot. Using the static dipole moment $ed = e \times 15.3 \pm 0.1 \text{ nm}$ [14] measured for the indirect exciton in our experiment, we obtain $\Delta E = 15.3 \pm 0.25 \text{ meV}$, fully consistent with the expected orbital energy spacings of similar QDs.

We continued to investigate the ultrafast dynamics of charge carriers in the QDM using pump-probe experiments with PC readout. Whilst details of the setup used are described in ref. [15] it provides, two independently tunable, transform limited picosecond laser pulse trains derived from a broadband femtosecond Ti:Sapphire source. After resonantly exciting the QDM with the pump pulse the photocurrent I induced by the time-delayed probe pulse is measured with a lock-in amplifier. Blocking and unblocking the pump beam reveals the *pump induced* change of the PC, ΔI . The quantities I and ΔI can be interpreted as the absorption by the QDM at the probe photon energy and its change induced by the pump pulse, respectively. Typical examples

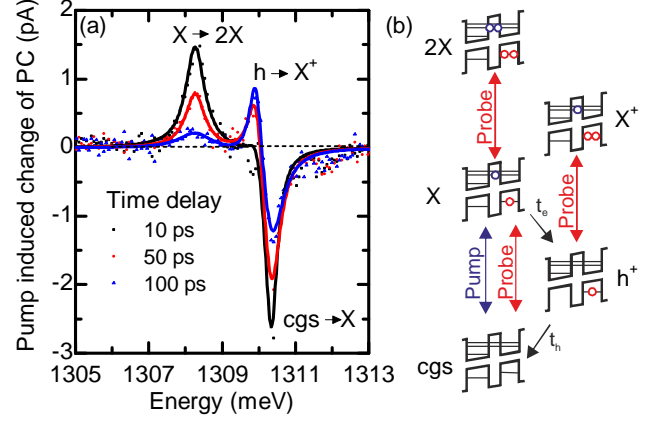


FIG. 2. (Color online) (a) Pump induced change of the probe induced photocurrent for various time delays elapsed since excitation. (b) Level scheme for the pump-probe experiments on the QDM.

of pump-probe PC spectra recorded away from the anti-crossings (at $F = 32.4 \text{ kV/cm}$) and three different time delays $t_D = 10, 50$ and 100 ps are presented in Fig.2(a). To record these pump probe spectra, the pump pulse was fixed to the direct neutral exciton in the upper dot X at 1310.3 meV . The figure clearly exhibits two positive going resonances (pump induced absorption) at 1308.3 meV and 1309.9 meV , respectively. In addition, a pronounced negative going dip (pump induced bleaching) is observed at the energy of X at 1310.3 meV . The observed pump-probe spectra are similar to those observed in single dot experiments [15–17] and can be understood with the level scheme depicted schematically in Fig.2(b). The pump pulse generates an exciton in the upper QD and, providing that the time delay between pump and probe is less than the tunneling timescales for electron and hole tunneling, the probe pulse can further excite the system to generate the spatially direct biexciton. This explains the pronounced pump induced absorption peak $X \rightarrow 2X$ at 1308.3 meV , red-shifted by 2 meV from the exciton transition $cgs \rightarrow X$. As the time delay increases, carriers tunnel out of the upper dot with the tunneling time of the electron t_e with its smaller effective mass being much shorter than that of the hole (t_h). If the electron tunnels out of the upper dot, leaving it occupied by a single hole the system exhibits an induced absorption peak at the $h \rightarrow X^+$ transition (peak at 1309.9 meV). The anticorrelated intensity of $X \rightarrow 2X$ and $h \rightarrow X^+$ can clearly be observed in Fig.2 as t_D increases from 15 to 100 ps. If pump and probe pulse are both centered at the exciton transition $cgs \rightarrow X$, the probe pulse detects a bleaching of the exciton, resulting in the strong negative signal ΔI observed in Fig.2(a).

To quantitatively analyze electron and hole tunneling, the pump photon energy is fixed to the $cgs \rightarrow X$ tran-

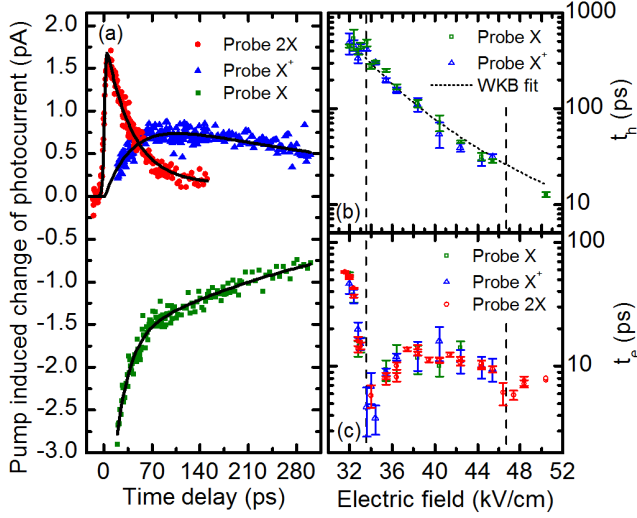


FIG. 3. (Color online) (a) Temporal evolution of PC change ΔI probing the resonances identified in Fig.1(c). (b) Hole and (c) electron tunneling times t_h and t_e as a function of the applied electric field F .

sition, while the probe photon energy is tuned to the three resonances identified in Fig.2(a). For each curve in Fig.3(a) ΔI is presented as a function of t_D , for probe pulses tuned to the $cgs \rightarrow X$ (green squares), $h^+ \rightarrow X^+$ (blue triangles) and $X \rightarrow 2X$ (red circles) transitions, respectively. Fits to each set of data using a rate equation model that accounts for sequential electron and hole tunneling [15] (lines in Fig.3a) show very good global agreement with all of the measured data and permit the direct (and independent) determination of t_h and t_e . To investigate the influence of the coupling presented in Fig.1, detailed studies were performed over the range of electric field $31 \text{ kV/cm} \leq F \leq -51 \text{ kV/cm}$ encompassing the anticrossing presented in Fig.1. The obtained values of t_h obtained with the probe pulse tuned to the $cgs \rightarrow X$ (green squares) and the $h^+ \rightarrow X^+$ (blue triangles) transition are presented in Fig.3(b). Similarly, the field dependence of t_e extracted by probing either the $cgs \rightarrow X$ (green squares - Fig.3c), $h^+ \rightarrow X^+$ (blue triangles) and $X \rightarrow 2X$ (red circles) transition are plotted in Fig.3(c). In all cases, the tunneling times obtained by probing the different transitions are in excellent agreement with each other supporting the overall validity of the interpretation and the level scheme used (Fig.2(b)) over the whole range of F analyzed here. The hole tunneling time monotonically decreases from $t_h = 450 \text{ ps}$ at $F = 32 \text{ kV/cm}$ to $t_h = 12.6 \text{ ps}$ at $F = 50.5 \text{ kV/cm}$ and exhibits a clear $\exp(-1/F)$ dependence. This behaviour can be explained with WKB theory with the tunneling rate Γ [18]

$$\Gamma = \frac{16V_s^2 L}{\pi^2 \hbar^2} \sqrt{\frac{m_s^*}{2|E_s|}} \exp \left[-\frac{4\sqrt{2m_s^*}}{3\hbar e F} |E_s|^{\frac{3}{2}} \right] \quad (1)$$

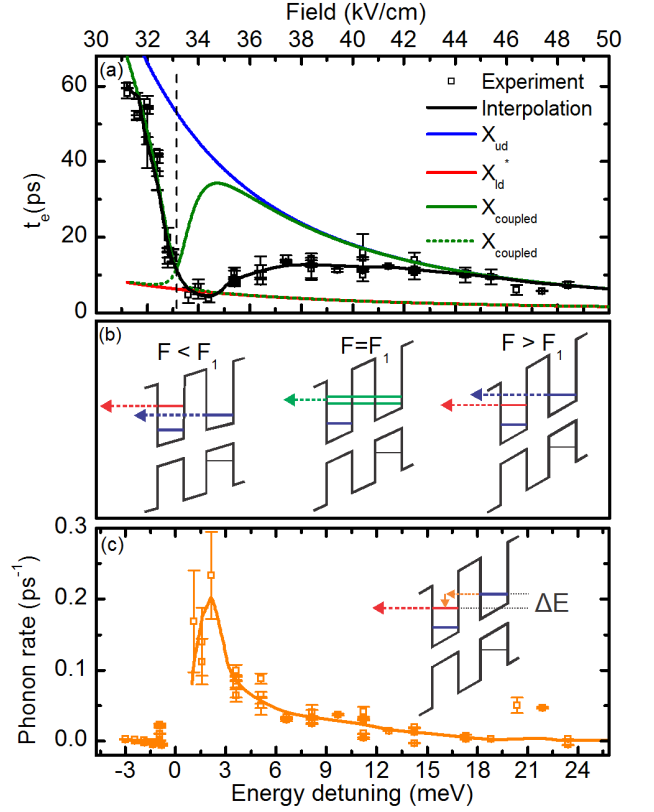


FIG. 4. (Color online) (a) Tunneling time of the electron t_e . Measured data is shown as points. Theoretical analysis of the tunneling times of e_{ud} (e_{id}^*) is presented as a blue (red) line and for the coupled case as green lines. (b) Schematic illustration of the alignment and tunneling of e_{ud} and e_{id}^* (c) Phonon rate extracted from (a)

where m_s^* is the effective mass of the particle s (electron or hole), L and V_s are the width and effective depth of the potential well and E_s is the single particle energy. A fit to the experimental data using eq. 1 is presented as a dashed line in Fig.3(b) and consistently reproducing the experimental data. The reason that $t_h(F)$ exhibits a behavior that can be accounted for by WKB theory is related to the fact that the hole tunnels through an approximately triangular potential barrier without any influence of the lower QD (see Fig.2). In marked contrast, the field dependence of t_e (Fig.3c) exhibits significantly richer behavior. Whilst t_e also decreases with F as expected, we also observe a series of resonances marked with dashed lines on Fig.3(c) where t_e becomes comparable to the pulse duration of the probe laser pulse (3 ps). The most pronounced resonance occurs at $F_1 = 33.1 \text{ kV/cm}$ precisely where the anticrossing presented in Fig.1 occurs. A second, weaker, dip of t_e is observed at $F_2 = 46.5 \text{ kV/cm}$ where e_{ud} anticrosses with the second excited orbital state of the electron in the lower dot e_{id}^{2*} (PC data not presented).

In the following, we present a detailed analysis of the

ultrafast electron tunneling in the vicinity of the anticrossing at $F_1 = 33.1 \text{ kV/cm}$ and show that it results from tunneling between the two dots forming the molecule with and without the participation of phonons. The electron tunneling time t_e as a function of F is plotted in Fig.4(a) on a linear scale, the position of the anticrossing is indicated by the vertical dashed line. In our theoretical analysis we consider tunnel processes according to eq. 1 for the two electron levels involved in the anticrossing e_{ud} and e_{ld}^* , as schematically depicted in blue and red in Fig.4(b). Since the two dots forming the QDM are similar in size and electronic structure, we assume identical confinement potentials for e_{ud} and e_{ld} . As discussed above, e_{ld}^* lies 15.3 meV to higher energy than e_{ld} , reducing the effective tunnel barrier. Thus, generically we expect electron tunneling out of the lower dot into the continuum to be faster from e_{ld}^* compared with e_{ld} . When the two dots are coupled by tunneling (e.g. for $F = F_1$ - Fig.4(b)) the Hamiltonian is $\mathbf{H} = \mathbf{H}_0 + \mathbf{V}_1$, where \mathbf{H}_0 is the Hamiltonian of the detuned system and the coupling term \mathbf{V}_1 is measured from the PC data shown in Fig.1. The effective broadening of the coupled states is then given by the imaginary part of the eigenvalues of the coupled eigenstates $\epsilon_i = E_i - i\Gamma_i$

$$2\epsilon_{\pm} = \epsilon_{ld^*} + \epsilon_{ud} \pm \sqrt{(\epsilon_{ld^*} - \epsilon_{ud})^2 + 4V_1^2} \quad (2)$$

Far from resonance the tunnel rates from e_{ud} can be fitted using WKB formalism. This results in the blue (red) curve for e_{ud} (e_{ld}^*) presented in Fig.4(a), taking only the measured energy difference between e_{ld} and e_{ld}^* of 15.3 meV into account. At resonance the levels are mixed by tunneling and the decay rates of the coupled states exchange character with an intersection at F_1 . The corresponding calculated values of t_e are presented as green lines in Fig.4(a). For all electric fields we pump the state which is more located in the upper QD (solid green line), resulting in a dip of t_e at F_1 . The theoretical model quantitatively explains the measured values of t_e for $F < F_1$ and $F \gg F_1$. However, pure resonant tunneling would give rise to a much narrower resonance (green curve - Fig.4) than is observed experimentally. In experiment, the resonance is asymmetrically broadened for $F > F_1$. Closer inspection even shows that the shortest time t_e is not observed at F_1 as expected from the theory but shifted by $\Delta F = +1 \text{ kV/cm}$ to 34.1 kV/cm . These clear experimental observations show that an additional mechanism must be active to shorten t_e for $F_1 < F < 41 \text{ kV/cm}$ and produce the asymmetric resonance observed (Fig.4a).

We continue to present evidence that this mechanism is acoustic phonon mediated inelastic inter-dot tunneling into e_{ld}^* . First, we compute the decay rate of an additional scattering mechanism from the difference between the measured tunneling times t_e (black curve - Fig.4(a)) and the expected one from the model based

on eq. 2 (green curve). Taking into account the measured static dipole moment $ed = e \times 15.3 \pm 0.1 \text{ nm}$ of the indirect exciton the additional decay rate can be obtained as a function of the energy detuning between the tunnel-coupled states. The result of this analysis is plotted in Fig.4(c) revealing a clear maximum for a positive detuning of $+1.7 \pm 0.1 \text{ meV}$ from resonance and a rate that is below experimental error for negative detunings. This characteristic energy scale of a few millielectronvolts corresponds to the energy of acoustic phonons in GaAs with a wavelength comparable to the QD size as well as the interdot distance within the QDM [19]. Theoretical calculations of the coupling between molecular states and phonons in similar structures (with 12 nm separation between the dots) taking into account deformation- and piezoelectric- exciton-phonon coupling reported a spectral density which shows a maximum around 1.4 meV with a rate of 0.3 ps^{-1} [19]. We interpret the additional relaxation channel as reflecting phonon mediated inelastic tunneling between the two dots forming the molecule, as schematically depicted in the inset of Fig.4(c). For positive detunings of e_{ld}^* the electron tunnels into e_{ld}^* whilst simultaneously emitting a phonon with an energy equal to the level separation. From there it most likely tunnels out of the excited orbital state of the QDM instead of relaxing to the ground state since the tunneling escape time from the excited state is $< 5 \text{ ps}$ (see red line in Fig.4(a)). In contrast, for negative detunings where phonon absorption would be required, such an inelastic tunneling is prohibited by the negligible phonon occupation at the lattice temperature used for the measurements presented here. To further corroborate this interpretation we performed measurements of t_e at an elevated temperature of $T = 50 \text{ K}$. For the case of phonon emission (e_{ld}^* red detuned compared with e_{ud}) t_e remained the same for all measurements. In contrast, for the case of phonon absorption (e_{ld}^* blue detuned) we typically observe a strong decrease of t_e [20]. This strongly supports the model of phonon-mediated inelastic tunneling to the excited orbital state of the lower dot.

In summary, we investigated few-Fermion dynamics in a QDM using ultrafast pump probe spectroscopy with PC readout. We determined the electron and hole tunneling times as a function of F and showed that t_e shows resonances when the electron is coupled to excited orbital states of the lower dot. In this regime, the tunnel coupled energy level serves as an intermediate state facilitating electron escape within several ps. For the case of slightly detuned electronic levels within the QDM, inelastic tunneling involving the emission of acoustic phonons is found to govern the tunnel dynamics out of the QDM.

We gratefully acknowledge financial support of the DFG via SFB-631, Nanosystems Initiative Munich and the Emmy Noether Program (H.J.K.), the EU via SOLID and the TUM Graduate School.

* finley@wsi.tum.de

- [1] S. De Franceschi, S. Sasaki, J. M. Elzerman, W. G. van der Wiel, S. Tarucha, and L. P. Kouwenhoven, *Phys. Rev. Lett.* **86**, 878 (2001).
- [2] H. Qin, A. Holleitner, K. Eberl, and R. Blick, *Phys. Rev. B* **64** (2001), 10.1103/PhysRevB.64.241302.
- [3] N. Mason, M. J. Biercuk, and C. M. Marcus, *Science* **303**, 655 (2004), <http://www.sciencemag.org/content/303/5658/655.full.pdf>.
- [4] H. J. Krenner, M. Sabathil, E. C. Clark, A. Kress, D. Schuh, M. Bichler, G. Abstreiter, and J. J. Finley, *Phys. Rev. Lett.* **94**, 057402 (2005).
- [5] E. Stinaff, M. Scheibner, A. Bracker, I. Ponomarev, V. Korenev, M. Ware, M. Doty, T. Reinecke, and D. Gammon, *Science* **311**, 636 (2006).
- [6] H. J. Krenner, E. C. Clark, T. Nakaoka, M. Bichler, C. Scheurer, G. Abstreiter, and J. J. Finley, *Phys. Rev. Lett.* **97**, 076403 (2006).
- [7] A. S. Bracker, M. Scheibner, M. F. Doty, E. A. Stinaff, I. V. Ponomarev, J. C. Kim, L. J. Whitman, T. L. Reinecke, and D. Gammon, *Appl. Phys. Lett.* **89**, 233110 (2006).
- [8] M. Scheibner, M. Yakes, A. S. Bracker, I. V. Ponomarev, M. F. Doty, C. S. Hellberg, L. J. Whitman, T. L. Reinecke, and D. Gammon, *Nature Physics* **4**, 291 (2008).
- [9] M. F. Doty, M. Scheibner, I. V. Ponomarev, E. A. Stinaff, A. S. Bracker, V. L. Korenev, T. L. Reinecke, and D. Gammon, *Phys. Rev. Lett.* **97**, 197202 (2006).
- [10] W. Liu, S. Sanwlani, R. Hazbun, J. Kolodzey, A. S. Bracker, D. Gammon, and M. F. Doty, *Phys. Rev. B* **84**, 121304 (2011).
- [11] J. M. Elzerman, K. M. Weiss, J. Miguel-Sanchez, and A. Imamoglu, *Phys. Rev. Lett.* **107**, 017401 (2011).
- [12] T. Nakaoka, E. C. Clark, H. J. Krenner, M. Sabathil, M. Bichler, Y. Arakawa, G. Abstreiter, and J. J. Finley, *Phys. Rev. B* **74** (2006), 10.1103/PhysRevB.74.121305.
- [13] K. C. Wijesundara, J. E. Rolon, S. E. Ulloa, A. S. Bracker, D. Gammon, and E. A. Stinaff, *Phys. Rev. B* **84**, 081404 (2011).
- [14] K. Müller, G. Reithmaier, E. C. Clark, V. Jovanov, M. Bichler, H. J. Krenner, M. Betz, G. Abstreiter, and J. J. Finley, *Phys. Rev. B* **84**, 081302 (2011).
- [15] M. Zecherle, C. Ruppert, E. C. Clark, G. Abstreiter, J. J. Finley, and M. Betz, *Phys Rev B* **82**, 125314 (2010).
- [16] A. J. Ramsay, S. J. Boyle, R. S. Kolodka, J. B. B. Oliveira, J. Skiba-Szymanska, H. Y. Liu, M. Hopkinson, A. M. Fox, and M. S. Skolnick, *Phys. Rev. Lett.* **100** (2008), 10.1103/PhysRevLett.100.197401.
- [17] S. J. Boyle, A. J. Ramsay, F. Bello, H. Y. Liu, M. Hopkinson, A. M. Fox, and M. S. Skolnick, *Phys. Rev. B* **78** (2008), 10.1103/PhysRevB.78.075301.
- [18] J. Villas-Boas, S. Ulloa, and A. Govorov, *Phys. Rev. Lett.* **94** (2005), 10.1103/PhysRevLett.94.057404.
- [19] K. Gawarecki, M. Pochwała, A. Grodecka-Grad, and P. Machnikowski, *Phys. Rev. B* **81**, 245312 (2010).
- [20] For example for a detuning of $\Delta E = -1.33\text{meV}$ we observe a reduction of t_e from $42.5 \pm 2\text{ps}$ to $26 \pm 2\text{ps}$ and at $\Delta E = -2.4\text{meV}$ from $58 \pm 2\text{ps}$ to $34 \pm 3\text{ps}$.